ANALYSIS OF OPEN-PIT MINING ACTIVITIES
USING SENTINEL-1A/B COHERENCE IMAGERY

Jihyun Moon (1), Hoonyol Lee (1)

[1] Kangwon National Univ., 1 Kangwondaehak-gil, Chuncheon-si, Gangwon-do, 24341, Korea
Email: answlgus12@kangwon.ac.kr, hoonyol@kangwon.ac.kr

KEY WORDS: Musan mine, InSAR coherence, NDAI

ABSTRACT: Open-pit mining is one of the surface mining technique extracting minerals from the surface. As open-pit mines are often rock fields with sparse vegetation, Interferometric Synthetic Aperture Radar (InSAR) technique can be used effectively. InSAR coherence detects random surface change that measures the activity or stability of the surface using interferometric phase data. High coherence will be maintained on the surface where there is no movement and only surface scattering. On the other hand, the surface where there is a lot of movement and volumetric scattering has low coherence value. Therefore, using 12-day InSAR coherence images from Sentinel-1A/B satellites, for example, it is possible to analyze how active the open-pit mine is during the 12 days. The Musan mine in North Korea is the largest open-pit iron mine in Asia with the proved reserves of about 2.06 billion tons and more than 9 square kilometers. We used a total of 102 SAR images of Sentinel-1A/B distributed freely from European Space Agency (ESA) from June 2015 to April 2019 and over 100 scenes of 12-day InSAR coherence data were obtained. Stable and moving spots were selected through the average and standard deviation of the entire coherence time series data. Coherence values include not only the mining activity but also the effects of perpendicular baseline, temporal baseline, and weather condition. Therefore, Normalized Difference Activity Index (NDAI) is newly defined to remove the noise and only the coherence variation due to the influence of the mining activity was extracted. Observation shows various mining activities in time. This is a preliminary study that can be verified through comparison with other relevant data such as seismic or acoustic data.

1. INTRODUCTION

Economic mineral resources are mostly in large-scale ore deposits of which operation is mainly in open-pit mining (Yang *et al*., 2016). Vegetation is rarely distributed at the mining site because the topsoil is removed and the ore is mined directly from the surface. Therefore, it is effective to observe surface displacement at the mining site using Interferometric Synthetic Aperture Radar (InSAR) technology. InSAR technology enables accurate measurement of the surface displacement between two SAR images of the same area in less than a centimeter accuracy.

InSAR coherence detects random surface change that measures the activity or stability of the interferometric phase of InSAR data. High coherence will be maintained on the surface where there is no movement and only surface scattering. On the other hand, the surface where there is a lot of movement and volumetric scattering has low coherence value (Lee, 2006) Therefore, the InSAR coherence value is low when mining activity is in progress on the surface. This study uses InSAR coherence to analyze the activity of the mine that cannot be investigated easily in the field.

The study area of this research is the Musan Mine in North Korea near the border with China (Fig. 1). The amount of confirmed reserves is about 2 billion tons. The quality of ore is known to be 25-35% and the quality of concentrate is 65%. (Nam, 2014)

Figure 1. The study area: Musan Mine.(left: Map from Asiapress, right: Map from Google Earth.)

Sentinel-1 data are freely available as part of the ESA Copernicus program. The Sentinel-1 satellites are equipped with C-band radar and offer near global coverage. (Geudtner *et al*, 2014) Sentinel-1A was launched in 2014 and Sentinel-1B in 2016. Both satellites have Sun-synchronous orbits, 693 km above the Earth, and acquire SAR images of the same area every 12 days. SAR technology produces high-quality surface images without being affected by weather conditions, light levels and solar altitude.

For this study, Single Look Complex (SLC) data were acquired using the Interferometric Wide Swath (IW) Mode from the descending track. The IW has a wide swath of 250 km and the spatial resolution is 5 m in range and 20 m in azimuth directions. The SLC is a complex data containing the phase and amplitude information in slant range and azimuth coordinates.

Sentinel-1A satellite images were acquired from June 11, 2015 to May 24, 2016, followed by Sentine-1B satellite images from September 27, 2016 to April 21, 2019. A total of 102 SAR images were downloaded from ESA portal. There is a gap between May 24 and September 27, 2016 due to the transition of the data acquisition plan.

2. METHODS

2.1 InSAR Processing Chain
The SNAP program was used to process Sentinel-1A/B data. The SNAP program is a satellite image data processing program developed by ESA. S1TBX (Sentiel-1 Toolbox), an open source toolbox for Sentinel-1A/B data processing, provides the whole image processing chain in user-friendly environment.

First, the algorithm was constructed using the graph builder (Fig. 2) to perform the SAR interferometry to obtain a coherence map and interferogram.
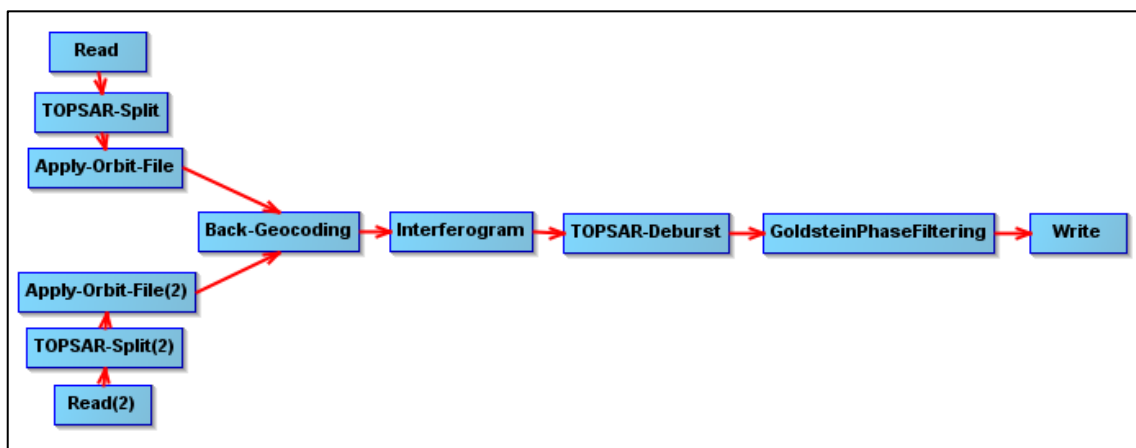
Figure 2. Interferometric SAR Algorithm in Graph Builder of SNAP program.

In Fig. 2, Read is a step of loading SAR Image: Master image is input to Read and Slave image is to Read(2). In the TOPSAR-Split and TOPSAR-Split(2) steps, IW2 swath image containing Musan Mine is extracted out of the three swaths (IW1, IW2 and IW3) of SLC data. Also, three bursts out of nine that includes the Musan Mine were extracted. Apply-Orbit-File is the step to update the primary orbital state vector to the Sentinel Precise Orbit. The primary orbit, the initial orbital information at the time of data acquisition, has an error range of 10 ~ 20 cm. The Sentinel Precise Orbit which re-computes orbit information by combining astronomical data about two weeks after SAR imaging has a smaller error range of less than 10 cm. Next, external DEM data (SRTM 1 arc sec HGT DEM) is applied through the Back-Geocoding step. In this step, master image and slave image are used together and the geographical coordinates of both images are matched. In the Interferogram step, interferogram and coherence map is generated using the phase difference between the master image and the slave image. The flat-earth phase and the topographic phase due to the surface

altitude are removed. The coherence window size was applied by selecting range 7 and azimuth 2 so that the resolution of coherence image is approximately 40 m both in range and azimuth directions. The interval between bursts was eliminated through the TOPSAR-Deburst step. The Goldstein Phase Filtering step is applied to eliminate phase noise. Finally, the final image was extracted in BEAM-DIMAP format through the Write step. 100 SAR coherence map images were acquired sequentially using a total of 102 SAR images.

2.2 Terrain Correction

Terrain correction was performed on the coherence map obtained through InSAR data processing in SNAP. This process can also correct terrain distortions such as layover, foreshortening, and shadowing. Terrain correction allows you to project images onto other domains such as Google Earth. The position of the image matches the actual position, so that the orientation, size and length of the image can be accurately measured.
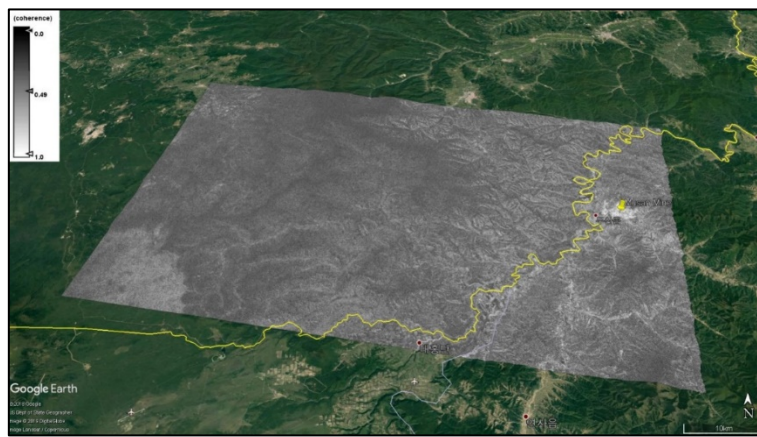
Figure 3. An example of InSAR Coherence Map with Terrain Correction (April 9-21, 2019)

2.3 Spatial Subset

When the InSAR coherence map with Terrain Corrections is projected onto the Google Earth domain, about 80% of the image area was located in China. (The yellow line in Figure3 represents the border. The northern part is China and the southern part is North Korea.) Through the Spatial Subset process in SNAP, only the mining area needed for this study was extracted based on Geo-Coordinates. The range of the mining area was set at 42.206 ~ 42.281 ° latitude and 129.211 ~ 129.324 ° longitude.
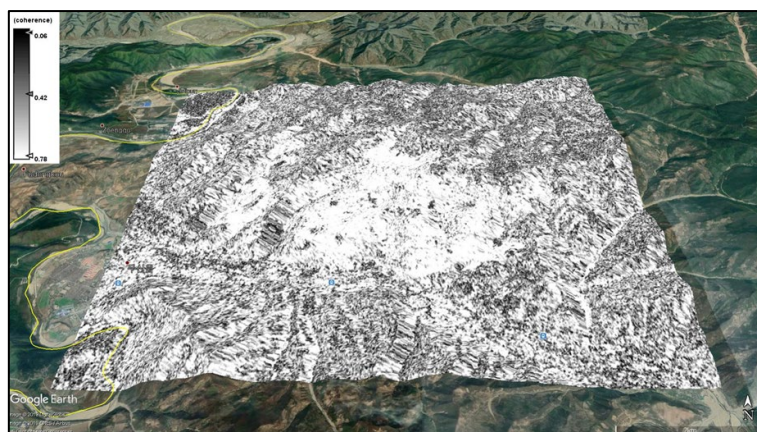
Figure 4. An example of InSAR Coherence Map with Spatial Subset (April 9-21, 2019)

2.4 Band Math (Average and Standard Deviation)

The Band Math provided by the SNAP program can be used to work with images that exist in one file. Therefore, by using collocation, all coherence images are combined into one file with the same topographical coordinates. The average and standard deviation of the whole coherence images were calculated to identify the stable area and to access the quality of the data.

2.5 12-day Coherence

2.5.1 Target Spots:
Target spots were selected to confirm changes in InSAR coherence at 12-day intervals. Based on the high resolution imagery of the Google Earth domain, the region where the location of the mining equipment is identified is selected as a target spot candidate. Because of the high probability of finding traces of mining, the location of mining equipment can be used to predict the mining area. 12-day InSAR coherence images were also checked along with the location of the mining equipment. The final target spots were determined where the coherence decreased in the candidate sites.
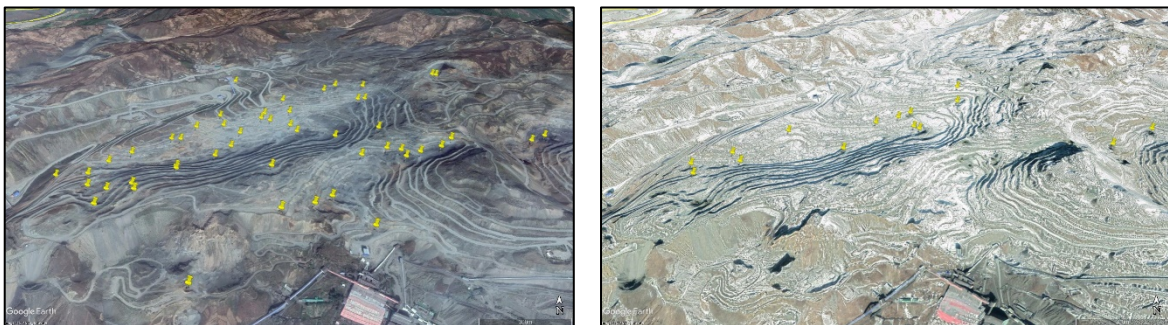
Figure 5. Location of Mining Equipment (left:22 Sep 2017, right:14 Feb 2019 images on Google Earth)

For example, Target 1 was confirmed through a Google Earth imagery taken on February 14, 2019. Unlike the surrounding area, there was no snow accumulated near the target point. Therefore, it was determined that snow was removed by mine activities, and it was selected as a target spot. The 12-day InSAR coherence image, which calculated the phase difference between February 18, 2019 and February 20, 2019, showed that the coherence of the target point decreased. Target 1 was finally determined as the target spot.
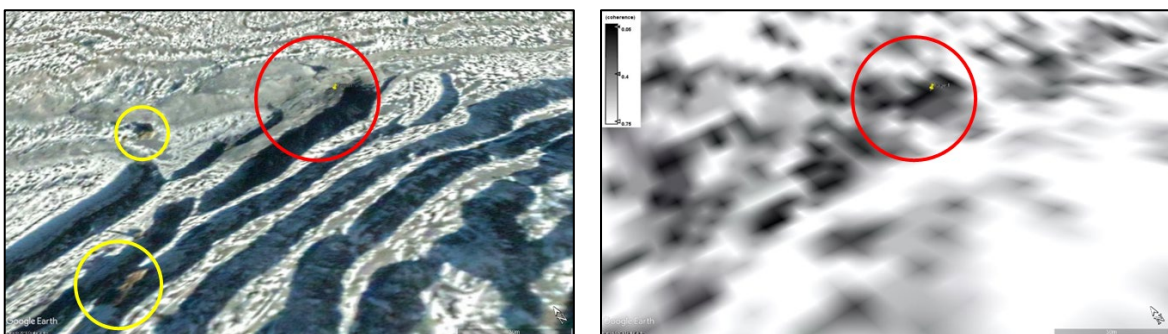
Figure 6. Google Earth Imagery (left) and Coherence Map (right, Feb. 8-20 Feb 2019).
Target 1 (red circle) and Mining Equipment (yellow circle)

The 12-day InSAR coherence change in Target 1 was plotted. InSAR coherence acquired at 24 and 36 day intervals is indicated by red dots.
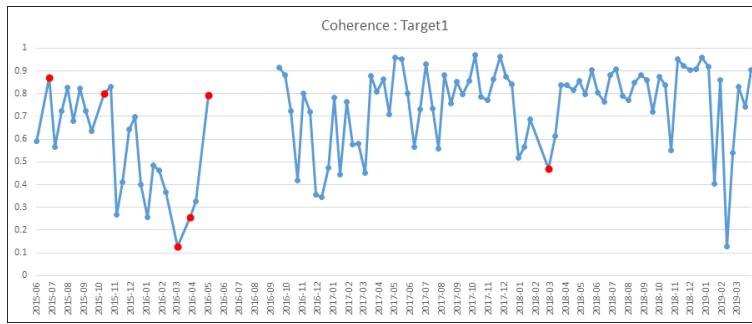
Figure 7. Coherence Change in Target 1

Coherence change graphs suggest that land surface changes have continued to occur, but we are not sure if the cause of this change is due to mining activity. Therefore, further analysis needs to be compared with other data that can confirm the mining activity.

2.5.2 Stable Spots:
Stable spots to be compared with target spots were selected using the average and standard deviation of 100 InSAR Coherence data. Band Math was used to extract the pixel with the highest average value and the lowest standard deviation value. The coherence average was about 0.92852 and the standard deviation was 0.07748. This point represents the most stable coherence value.
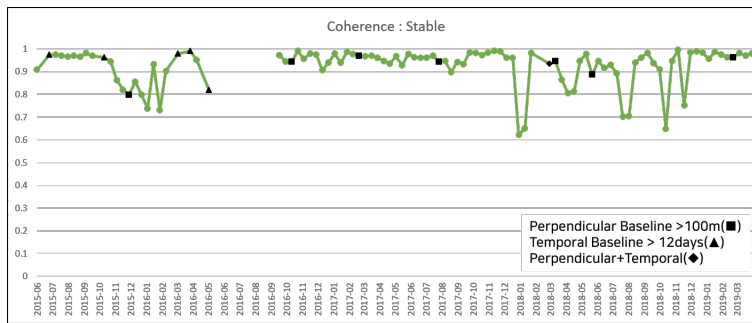
Figure 8. Coherence Change in Stable

We then examined the effect of the perpendicular baseline on the stable spot. In order to compare the coherence value with a value between 0 and 1, the perpendicular baseline (B) was divided by 100 m and the absolute value was taken and shown in the graph in Fig. 10. When comparing the period where the perpendicular baseline is over 100 m, that is, the value over 1 in the graph, and the section in which the coherence decreases rapidly, it was difficult to conclude that baseline had a significant effect on the reduction of coherence.
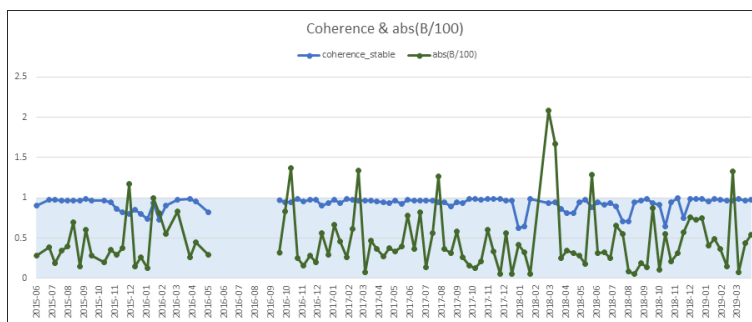
Figure 9. Coherence and Perpendicular Baseline Change in Stable

2.5.3 NDAI (Normalized Difference Activity Index):
There are many causes of phase decorrelation that affect coherence (Zebker and Villasenor, 1992). This study defined the coherence as follows.

$$\rho = \rho_{activity} \cdot \rho_{noise} = \rho_{activity} \cdot \rho_{perp\ baseline} \cdot \rho_{temp\ baseline} \cdot \rho_{weather} \tag{1}$$

Here, the NDAI (Normalized Difference Activity Index) was defined as follows to remove the coherence change

5

caused by noise and to express the coherence value as an index representing the active state of mining activity.

$$\text{NDAI} = \frac{\rho^{stable} - \rho^{target}}{\rho^{stable} + \rho^{target}} = \frac{\rho_{\text{activity}}^{stable}\rho_{noise}^{stable} - \rho_{\text{activity}}^{target}\rho_{noise}^{target}}{\rho_{\text{activity}}^{stable}\rho_{noise}^{stable} + \rho_{\text{activity}}^{target}\rho_{noise}^{target}} \quad (-1 < NDAI < 1) \qquad (2)$$

If $\rho_{noise}^{stable} \approx \rho_{noise}^{target}$, NDAI is expressed as

$$\text{NDAI} = \frac{\rho_{\text{activity}}^{stable} - \rho_{\text{activity}}^{target}}{\rho_{\text{activity}}^{stable} + \rho_{\text{activity}}^{target}} \qquad (3)$$

so that NDAI eliminates the effects of perpendicular baselines, temporal baselines, and atmospheric effects. Therefore, NDAI is an index that means only mining activity.
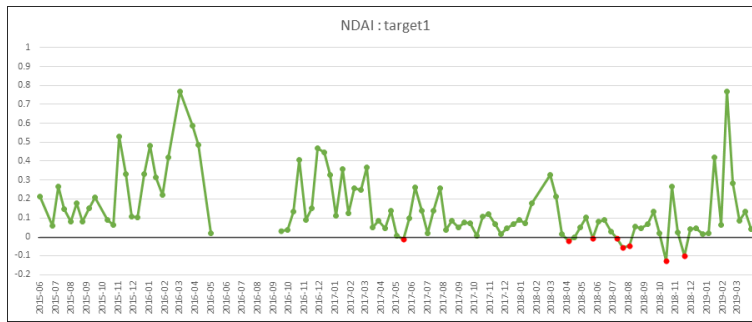
Figure 10. NDAI Change in Target 1(red dots: error)

In Fig. 11, the NDAI change in Target 1 data with a value less than 0 can be confirmed. The data where NDAI has a negative value indicates the coherence value at the stable point is smaller than that of the target. This is considered to be an error that cannot be theoretically established, and should be excluded for the interpretation.
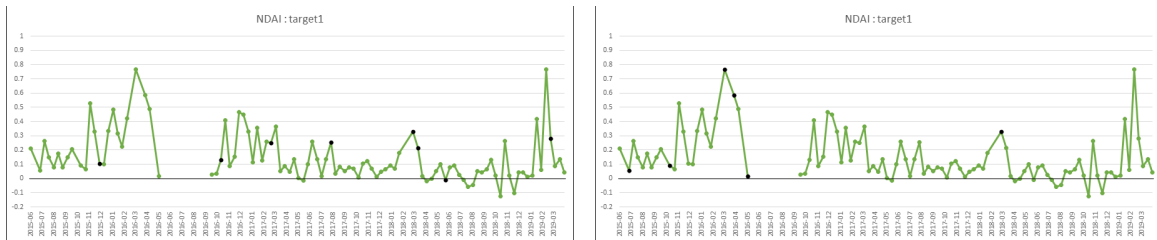
Figure 11. NDAI Change in Target 1
(left: the effects of the perpendicular baseline, right: the effects of the temporal baseline)

In Fig. 12(left), data with perpendicular baseline of more than 100m were marked with black dots to analyze the effect in left graph. When the perpendicular baseline is more than 100m, an error appears in one section. It can be concluded that the influence of the perpendicular baseline is effectively removed by the NDAI. Right one is a graph analyzing the effects of the temporal baseline marked with black dots on the sections that are not 12 days. There was no section where errors occurred when the temporal baseline is 24 and 36 days. The influence of temporal baseline can also be interpreted as effectively removed by NDAI.

In addition to the effect of the baseline, the cause of the error is an atmospheric effect. However, because the weather data for Musan could not be found, it could not be directly compared and confirmed. In addition, noise caused by conveyors located near the stable spot, and landslide on the surrounding slope can also cause errors.

Errors with negative NDAI accounted for less than 10% of the total 100 InSAR coherence data. The effect of the baseline has also been removed sufficiently. Therefore, it is more reliable to use the NDAI than to directly compare the coherence values.

3. RESULTS

6

3.1 Coherence Time Series

Three additional target spots were selected in the same way as the target 1 was selected (Fig. 14). Target 1 and Target 2 were selected based on the Google Earth image on February 14, 2019, and Target 3 and Target 4 were selected based on the Google Earth image on September 22, 2017. Mining activities were analyzed by NDAI analysis of the target spots (Fig. 15).

Figure 12. Target Spots and Stable Spot
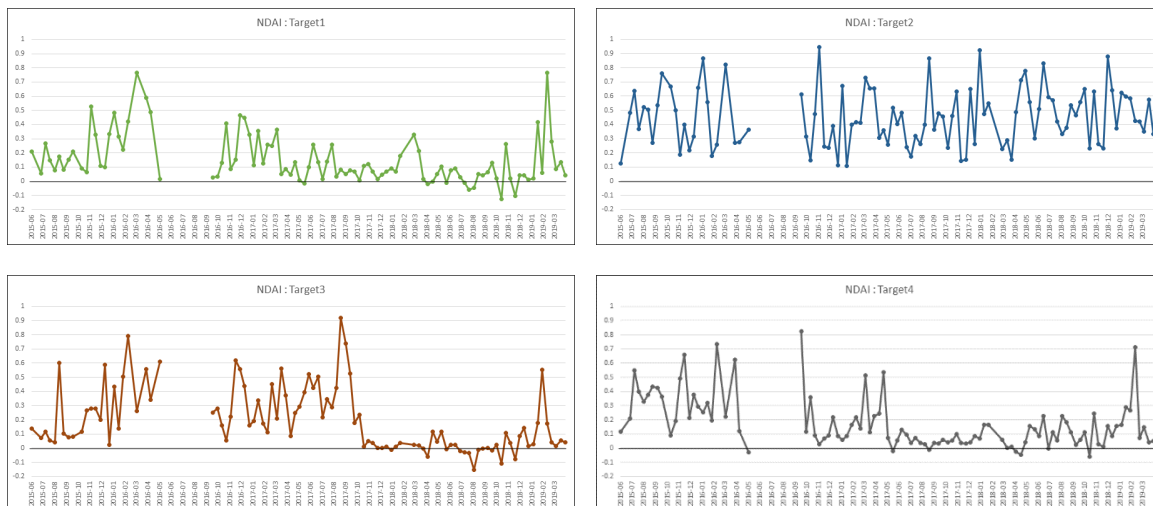
Figure 13. NDAI Change in Target 1, 2, 3 and 4.

Target 1 has a lower overall NDAI value compared to other Target spots. This spot has an active mining activities in 2015-17, after which activities diminished until February 2019 when the mining equipment appeared on Google Earth image. Target 2 has the largest average NDAI value, of which the surface change is also visible with the Google Earth images. Target 3 was active before November 2017, but since then, it has been remarkably stable. There has been little mining activity since November 2017, and as a result, many errors were observed as the NDAI approached zero. The largest period for NDAI is between August 29 and September 10, 2017. Target 4 was active before June 2017, and remains stable thereafter. The largest period for NDAI is between September 27 and October 9, 2016. Note that recent activities in early 2019 in all targets seems to be an error due to snow cover that has to be excluded for interpretation.

4. CONCLUSIONS

As a result of analyzing NDAI of four target spots, mining activities are underway at the Musan mine. The degree of activities can be observed by the time series coherence and NDAI images. However, it is not certain that mining activity has taken place using NDAI data alone. Since it is not known how much the NDAI value changes according to the mining of open pit mines, other references related to mining activities are required to analyze the mining activities in more detail.

5. REFERENCES

Hyung-Sik Yang et al., 2016, Surface Mining Engineering, CIR, Republic of Korea, pp.2-9

Hoonyol Lee, 2006, Investigation of SAR Systems, Technologies and Application Fields by Analysis of SAR-elated Journal Papers, Korean Journal of Remote Sensing, Vol.22, No.2, 2006, pp.153-174

Nam, S.Y, 2014, Development of Iron Ore from North Korea and Inter-Korean Cooperation, The Korean Journal of Unification Affairs, Vol.26, No.2, pp.75-113

Sungji Bae, Jaehyung Yu, Sang-Mo Koh, Chul-Ho Heo, 2015, 3D Modeling Approaches in Estimation of Resource and Production of Musan Iron Mine, North Korea, Economic and Environmental Geology, Vol.48, No.5, pp.391-400

Peak Chang-ryong, 2015, Musan Mine - Embezzlement of Wagon Fuel Widespread, Retrieved August 22, 2018, from http://www.asiapress.org.

Geudtner, D., Torres, R., Snoeij, P., Davidson, M., Rommen, B., 2014, Sentinel-1 System Capabilities and Applications., the 2014 IEEE International Geoscience and Remote Sensing Symposium (IGARSS), Quebec, QC, Canada, 13–18 July 2014, pp. 1457–1460.

Stephanie Olen, Bodo Bookhagen, 2018, Mapping Damage-Affected Areas after Natural Hazard Events Using Sentinel-1 Coherence Time Series, Remote Sensing, Vol.10, No.8, pp.1272

Zebker, H.A. and J. Villasenor, 1992. Decorrelation in Interferometric Radar Echoes, IEEE Transactions on Geoscience and Remote Sensing, Vol.30, No.5, pp.950-959